RICE UNIVERSITY

Pulsed Dye Laser For Excitation Of Strontium

by

Priya Gupta

A Thesis Submitted
in Partial Fulfillment of the
Requirements for the Degree

Masters of Science

Approved, Thesis Committee:

Thomas C. Killian, Chairman
Assistant Professor of Physics and
Astronomy

Barry F. Dunning
Sam and Helen Worden Professor of
Physics

Matthew G. Baring
Assistant Professor of Physics and
Astronomy

Houston, Texas

April, 2004

ABSTRACT

Pulsed Dye Laser For Excitation Of Strontium

by

Priya Gupta

This thesis describes the construction and characterization of a high energy, tunable, pulsed dye laser that is used to make ultracold strontium plasma. In order to make ultracold plasma, we cool and trap strontium atoms in a magneto-optical trap (MOT) and then photoionize them with the dye laser. The dye laser is pumped by high-energy 355nm pulses from a commercial Nd:YAG laser and it gives out 10ns pulses of 400-415nm light with up to 50mJ/pulse. We will discuss the lasers spectrum, wavelength calibration, output power and efficiency for photoionizing strontium.

Acknowledgments

I would like to dedicate this thesis to my family who, despite the obstacles, stood by my side and supported my decision of pursuing a phD in physics. My parents have always taught me to excel in whatever I do and that provides me with the motivation to work hard and be a good researcher. My brother has changed my outlook towards life and helped me become a better person. I would like to thank my advisor Professor Thomas Killian for his invaluable time and patience in answering my endless questions. His ability to be 'perfect' and always know the right thing to do has never ceased to amaze me. I am very grateful to Susan Cudnik for helping me find things when I am lost in the chemistry stockroom. I cannot thank my labmates enough for the encouragement and entertainment they provide at all times. Their help and support was a key element in the successful completion of my masters. Sampad has not just been a great labmate, but also a wonderful friend and brother. Since naming all my friends and their individual contributions would make a thesis in itself, all I can say in this acknowledgement is that I want to thank all my friends for making the world a better place to live in. Their constant attention and entertainment helped refresh my mind and prepare me for a new day at work. I want to thank Ben for putting up with my mood swings which followed the mood swings of my laser, thank you for always being there for me. Last but not the least, I want to thank Atul for being a wonderful friend.

Contents

Abstract iii

Acknowledgments iv

List of Figures vii

1 Introduction 1

1.1 Ultracold Neutral Plasmas 1

1.2 Creation of Ultracold Plasma 3

1.3 Implications for laser design 5

1.4 Outline 6

2 Laser design and construction 7

2.1 Theory Behind Dye lasers 7

2.2 Main components 9

2.2.1 Pumping source 9

2.2.2 Oscillator Cavity 9

2.2.3 Preamplifier 14

2.2.4 Amplifier 15

2.3 Dye Circulator 16

2.4 Computer control 18

3 Ionization of Strontium 20

3.1 Ionization Fraction versus Power 22

3.2 Ionization Fraction versus Wavelength 23

4 Characterization of the Laser 27

4.1 Beam Quality 27

4.2 Output Power 30

4.3 Rydberg Series 30
4.4 Future Plans and prospects 37

References **39**

List of Figures

1.1 Experimental set up for laser cooling and trapping 3
1.2 Energy level and excitation scheme of neutral strontium 4

2.1 Transitions in a dye molecule 8
2.2 The dye laser cavity 10
2.3 Diffraction grating efficiency curve 12
2.4 Longitudinal pumping 16
2.5 Calibration of the counter 18

3.1 Energy levels of strontium 21
3.2 MOT fluorescence signal 21
3.3 Ionization Fraction versus Power 22
3.4 Ionization fraction at different wavelengths 24
3.5 Autoionization peak 25

4.1 Beam waist measurement 28
4.2 Saturation curve of dye laser 29
4.3 Output Power from PDL vs. Wavelength 30
4.4 Rydberg levels 31
4.5 Linewidth of the dye laser 32
4.6 Shifts in the Rydberg peak at different plasma densities 33
4.7 Residue from the fit of the counter readings 36

Chapter 1
Introduction

Ultracold plasmas were first made at the National Institute of Standards and Technology (NIST) at Gaithersburg, Maryland in 1999 [1]. The recipe was to laser cool and trap [2] xenon atoms in a magneto-optical trap (MOT) and then photoionize them to make an ultracold plasma. They obtained a plasma density of 2×10^9 cm^{-3} with ion temperature as cold as 10μK and electron temperature of 100mK. The size of their atom cloud was 200μm while the Debye length could be as small as 500nm. Kulin et al. [3] observed plasma oscillations and studied the expansion of the plasma. The plasma oscillations gave an insight into the electron density distribution. Killian et al. [4] observed recombination between ions and electrons to form Rydberg atoms in an expanding ultracold plasma.

The creation of ultracold plasma opened up a whole new regime in the field of plasma physics. Theorists predict strong coupling [5] and phase transitions between gas-liquid-solid behavior in this temperature range. Kuzmin and O'Neil [6], Robicheaux and Hanson [7] and Mazevet et al. [8] have simulated the evolution of an ultracold plasma. They realized that three-body recombination (TBR) dominates at the low temperatures of ultracold plasma and explored the ion-ion and electron-electron correlations.

1.1 Ultracold Neutral Plasmas

What is a plasma? A plasma is a collection of charged particles, namely, ions and electrons. Plasma exists all around us in the atmosphere. Whenever lightning strikes, it ionizes the air and forms hot plasma. There is plasma in the sun's atmosphere, Earth's ionosphere and the hot stars. But all these plasmas are hot, with temperatures more than 1000K. There has been extensive study of plasma at temperatures ranging

from $10^3 - 10^6$K [9].

The uniqueness of the plasma that we make is that it is ultracold, ranging in temperature from 1K to 1000K. The behavior of plasma at the ultracold temperature regime has not been well studied so it is very exciting to explore the system under various experimental conditions.

An ultracold plasma expands on a timescale of 10μs. This expansion is driven by the pressure of the electron cloud. This expansion gradually leads to the disintegration of the plasma on a 100μs timescale.

The ions and electrons have different kinetic energies and the system is not in equilibrium. Although, they do not thermalize with each other within the timescale of the experiment, the ions and electrons do thermalize amongst themselves. By understanding the trends in thermalization of the plasma we can get a deeper insight into the dynamics of the ions and electrons.

Before thermalization starts, the ions and electrons are at a high potential energy and low kinetic energy. The ratio of the potential energy between adjacent charged particles to their kinetic energy is defined as the Coulomb coupling parameter Γ. Thus,

$$\Gamma = e^2/rk_BT \tag{1.1}$$

where e is the electronic charge, r is the inter-particle distance, k_B is Boltzmann constant and T is the temperature of the system.

The Coulomb coupling constant is an important parameter. When it is greater than one, the potential energy dominates and the charged particles move in highly correlated motion. This strong coupling can then lead to liquid and solid-like behavior.

Apart from interacting with their own species, the ions and electrons recombine to form Rydberg atoms. The predominant form of recombination at ultracold temperatures is TBR which involves the recombination of an ion and electron while a

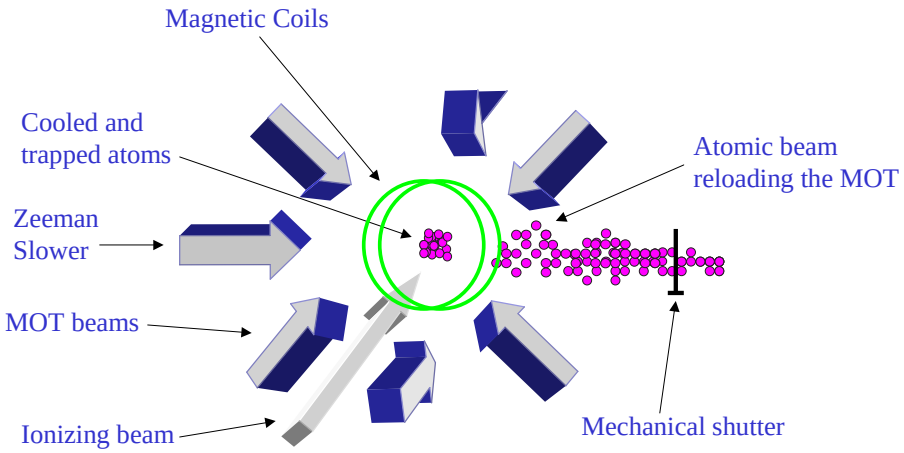

Figure 1.1 Experimental set up for laser cooling and trapping. The atoms are cooled to mK temperatures in the MOT with the help of the counter propagating zeeman beam, six MOT laser beams and magnetic coils. The mechanical shutter helps us block the atomic beam

second electron absorbs the energy released in the process of recombination. Thus, this process leads to heating of the electrons and hence the plasma.

Another interesting phenomena which connects Rydberg physics to ultracold plasma is the spontaneous evolution of Rydberg atoms into a plasma [10]. For the purpose of this thesis, we shall not discuss this in detail.

1.2 Creation of Ultracold Plasma

We use one of the strongest tools in AMO physics to cool and trap strontium atoms as shown in Figure 1.1: laser cooling and trapping [2]. We begin by slowing down an atomic beam with a counter propagating beam of light, called Zeeman slower, which is red detuned from the $^1S_0 - ^1P_1$ atomic transition at 460.862 nm. After slowing them to a velocity of about 50 cm/s, we use six counter-propagating laser beams, also red detuned, along with a properly oriented magnetic field, to trap the atoms and cool them to mK temperatures.

As shown in the Figure 1.2, laser cooling and trapping excites the atoms to the

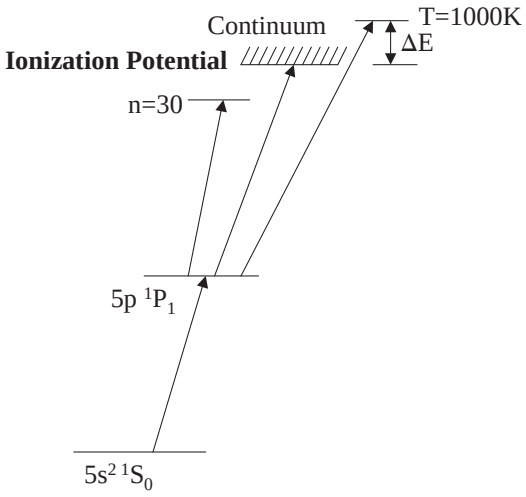

Figure 1.2 The 461 nm laser excites the atoms to the $^1P_1$ level. These excited atoms can then either be further excited to the Rydberg levels or ionized to form plasma. ΔE refers to the difference between the photon energy and the ionization energy

$^1P_1$ level. We then use a photoionizing laser to ionize these excited atoms. According to Esherick [11], the ionization energy of Sr^{88} is 45932.0 ±0.2 cm^{-1} and the energy required to excite a ground state atom to ^{1}P$_1$ level is 21698.47 cm^{-1}. Thus, the energy required to ionize a ^{1}P$_1$ level atom is 24227.13 cm^{-1}, which corresponds to a wavelength of 412 nm.

The energetics of an ultracold plasma created by this process is entirely dependent on the photoionization process and the initial density of the plasma. Just after the plasma is formed, the ions have the same kinetic energy as the laser cooled neutral atoms. Due to the difference in the mass of the ions and electrons, almost all the excess energy from the photoionizing laser, ΔE, is carried away by the electrons.

After the photoionizing process sets the initial energy of the electrons, the electrons collide with each other and thermalize within a nanosecond.

The ions take much longer to thermalize, typically hundreds of nanoseconds, due to their large masses. They start with a very high potential energy due to their disordered position in space. This disorder causes them to start moving, their potential

energy gets converted to kinetic energy, and they end up in a more ordered state with lower potential energy and higher kinetic energy. This is known as disorder induced heating. While the ions are thermalizing, some of the highly energetic electrons escape from the outer shell of the electron cloud. This causes a charge imbalance and creates a Coulomb well which traps the rest of the electrons. As mentioned earlier, the plasma expands due to electron pressure which causes the depth of the Coulomb well to decrease until all the electrons escape on a time scale of 100μs and the plasma disintegrates.

1.3 Implications for laser design

Equipped with the basic knowledge of how an ultracold plasma is formed, we can determine the requirement of a photoionizing laser. We want to study the dynamics of the plasma under various experimental conditions. One of the parameters we would like to vary is the initial kinetic energy of the electrons in the plasma. For this purpose, we need a tunable laser that can ionize the excited state atoms and take them far into the continuum. The wavelength of light that can excite the atoms up to a 1000K from the $^1P_1$ level is about 401 nm. Hence, we need a laser which can be tuned from 400 nm to 412 nm.

The Rydberg gas dynamics is very interesting due to processes like spontaneous ionization into a plasma. Hence, we want to make Rydberg atoms, by exciting one electron to the Rydberg levels. The energy required to excite the atom to n = 30 is 24104.52 cm^{-1}, which corresponds to a wavelength of 414.86 nm. Hence, in order to excite the atoms far in to the continuum as well as make Rydberg atoms, we need a laser which is tunable from 400 - 415 nm.

In order to study the dynamics of the plasma and the Rydberg gas, the photoionizing laser should be pulsed with pulsewidth of $\leq$ 10 ns. This is because we want to resolve the ion thermalization which occurs on a time scale of 100 ns within which

the ion temperature increases from a few mK to about 1K. The timescale over which the ions thermalize also depends on the plasma density.

Typically we trap about 1×10^8 Sr atoms in the MOT with peak density of about 3×10^{10} cm^{-3}. For favorable experimental conditions, we would like to photoionize atleast 30% of the neutral atoms to obtain peak plasma density on the order of 1×10^{10} cm^{-3}. The ionization fraction depends on the energy of the photoionizing laser, so to photoionize a good fraction of the excited atoms, we need a high-energy laser.

Not only do we want to excite a reasonable fraction of the atoms, we also want to monitor the energy to which they are excited. For our experiments, we can tolerate an error of up to 1K in the excitation energy of the plasma which corresponds to a bandwidth of about 20 GHz. This sets a goal for the linewidth of the photoionizing laser and the accuracy with which we can determine the wavelength.

Keeping all the requirements for the photoionizing laser in mind, a dye laser seems to be an apt system for the purpose. Thus, we decided to build a high energy, pulsed, tunable dye laser which is pumped by a high energy, pulsed Nd:YAG laser. The dye laser has proved to be a robust and reliable source of high energy, tunable light.

1.4 Outline

Chapter 2 follows with a detailed description of the design and construction of the dye laser. Chapter 3 talks about the ionization of strontium atoms using the dye laser. Results of the characterization of the beam quality, output power and linewidth of the laser are shown in Chapter 4 which ends with a note on the future work.

Chapter 2
Laser design and construction

2.1 Theory Behind Dye lasers

The key idea behind laser action is stimulated emission. A source of energy is needed to take the atoms from the ground state to an excited state. This pumping source can be an electrical source of energy, like in the case of diode lasers, or flash-lamps like in the case of our pulsed Nd:YAG laser or a laser light as in the case of dye lasers. Once the atoms are in the excited state, they can either decay through spontaneous emission, emitting a broad range of frequencies, or they can come down by stimulated emission in which case they emit a narrow bandwidth light. Stimulated emission dominates in a laser.

Stimulated emission from organic dyes was first observed in 1966 by three different groups, independently. Sorokin and Lankard [12] used a ruby laser to longitudinally pump their dyes whereas Schafer et al. [13] used a ruby laser for transverse pumping of their photosensitizing dyes. Spaeth and Bortfeld [14] also transversely pumped their organic dyes and studied shifts due to self-absorption. Soon extensive study on dye lasers began where possibilities of broad range wavelength control, high energy pulsed operation, narrow linewidths and ultrashort pulses were explored [15], [16], [17]. Soffer and McFarland [18] were the first to explore the use of a diffraction grating to obtain a continuously tunable and narrow band dye laser. Dye laser can be pumped by either a continuous wave or pulsed source. The wavelengths obtainable by various laser dyes range from UV to IR. A good introduction to dye lasers is [19].

The energy levels in dye molecules are broad. When pumped with a source of energy, the molecule is first excited to a higher level within the excited energy band. Through non-radiative processes, it comes down to a lower level within the energy band and eventually decays to the ground state through spontaneous emission. Thus

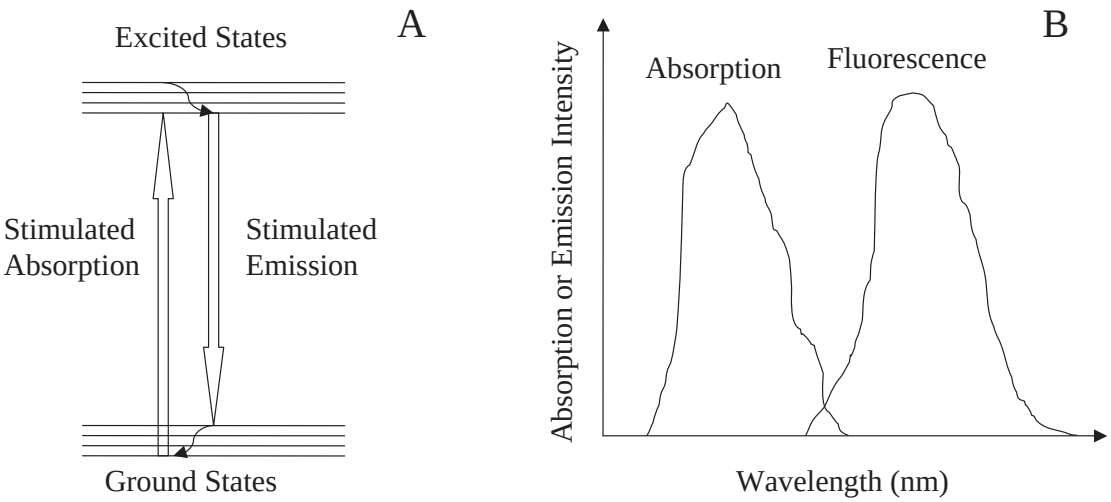

Figure 2.1 Figure A: Transitions in a dye molecule. The dye is excited from the ground state to excited state by stimulated absorption. There is non-radiative transition within the energy band and then the molecule comes down to the ground state by stimulated emission. Figure B: The absorbed wavelength is always shorter than the emitted wavelength in a dye molecule

the absorbed wavelength is always bluer than the emitted wavelength. The ground state is usually a singlet state so due to selection rules, the excited state is also a singlet state. Sometimes instead of decaying to the ground state, an excited electron decays to a metastable triplet state. Thus we always need a flowing dye to maintain fresh ground state molecules in the laser system.

When we think of building a dye laser, the first few considerations are the source of pump energy, the laser dye and solvent. The basic setup of a dye laser is well established and models are commercially available. Our dye laser is the PDL-1 from Quanta Ray that was graciously given to us by Carter Kittrell, Rice University. It required substantial work to adapt it to our specifications.

The laser is made up of three stages, the oscillator stage which forms the main laser cavity, and the preamplifier and amplifier stages that are just gain mediums. The various components in the laser are discussed in the next section.

2.2 Main components

2.2.1 Pumping source

To obtain population inversion, we use the third harmonic output of a high energy Nd:YAG laser as the pumping source. The laser puts out 240 mJ/pulse of 355 nm light. This pulsed laser has a repetition rate of 10Hz and a pulse width of 10ns. The beam is 1 cm in diameter and has a Gaussian profile.

Out of the 2.4W of pump light, we send about 10% to the oscillator stage, 10% to preamplifier stage and the rest to the amplifier. The beam splitters in the path of the pump beam are simply pieces of glass at 45° incidence angle that reflect 5% light from each surface and transmit the rest.

We observed that overdriving the oscillator dye makes the laser output power and beam shape unstable, so we pass the pump beam, going to the oscillator dye cell, through another beamsplitter that transmits only 50% of the light. The pump light then falls on the dye cuvet and excites all the molecules in its path.

2.2.2 Oscillator Cavity

The laser cavity is a very simple linear set up consisting of the gain medium, diffraction grating, beam expanders and an output coupler. The light coming out of the cavity is p-polarized. The polarization is determined by the polarization and orientation of the pump light.

The gain medium flows through a cuvet or cell, as it is often called, which is rectangular in shape and open from the top and bottom to allow the dye to flow through it. The opposite faces of the cuvet are wedged to keep them from acting as the input and output couplers of a laser cavity and thus preventing any lasing action within the cuvet itself. Although the faces of the cuvet have a very high damage threshold for UV through blue light, the adhesive used to stick the four faces does not. Thus if, due to misalignment, the laser light is concentrated on the adhesive,

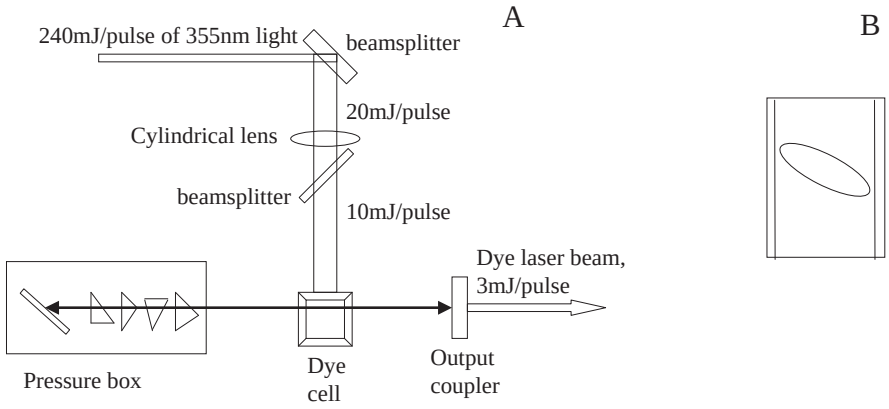

Figure 2.2 Figure A The dye laser cavity. The oscillator stage dye cell is transversely pumped. Figure B The pump beam is shaped as an elongated pattern when it hits the the dye cell

it will burn and damage the cuvet permanently. Thus one needs to be very careful while aligning the laser, especially when dealing with very high energy laser light.

To assist the alignment procedure, we passed a He-Ne beam through the laser such that it retraced the path that the light from the dye laser would follow. Hence, we could see the angle through which the beam is refracted by the walls of the dye cuvet and the path it would take within the dye cell. This greatly simplified the alignment of the dye laser.

We began the alignment by transversely pumping the oscillator stage dye cell. The pump beam is reflected by the two surfaces of a beam splitter as shown in Figure 2.2A to form an elongated pattern as can be seen in Figure 2.2B. The elongated beam then goes through a cylindrical lens of focal length 250 mm, which focuses it onto the dye cell at the angle obtained by the refraction of the He-Ne beam. The orientation of the cylindrical lens is an important alignment. The pump beam should be aligned such that the refracted dye laser beam goes through a region of excited molecules. In order to avoid burning the cell and overdriving the dye, the focus of the pump beam should not be tight. We positioned the cylindrical lens at a distance of about 220 mm from the dye cell and then slowly moved it closer to the cell until the output power

from the dye laser began to drop. Thus, we were able to find an optimal position for the lens.

The advantage of using transverse pumping is the ease of alignment and a large interaction region. The disadvantage of transverse pumping is poor beam quality. Due to the high absorption of the pump beam in the dye, the pump beam travels only a small distance of about a 100 microns into the dye before it is completely absorbed. Thus the laser beam travels very close to the edge of the dye cell and a lot of edge effects can be seen in the beam in the form of a diffraction pattern.

For our purpose, the advantages of transverse pumping override the disadvantages at the oscillator stage of the dye laser. However, a high-energy beam constitutes only one of the requirements from our dye laser. As explained in the last chapter, we also want the laser light to be tunable so that we can ionize Sr atoms, go far into the continuum and also excite Rydberg atoms. In order to obtain this tunability, we use a diffraction grating in the laser cavity. The grating sits on a rotating mount so as we tune the angle of the grating, the wavelength of light going back into the oscillator cavity is tuned. We used a plane ruled grating with 600 grooves/mm, and a nominal blaze angle of 54° to obtain a high reflectivity in the 7th order. We send the 7th order of the grating back into the laser cavity to obtain a greater resolution. The maximum resolution we can obtain from the grating, which is in Littrow configuration, with N number of grooves illuminated and a spacing d between the grooves, such that N*d is the length of the grating, is:

$$\frac{\lambda}{\Delta\lambda} = R_{max} = \frac{2 * N * d}{\lambda} = 2.72 * 10^6 \tag{2.1}$$

where $\lambda = 412 \times 10^{-9}$ is the wavelength of light and $\Delta\lambda$ is the bandwidth of light in the 7th order. Therefore, $\Delta\lambda = 6.6$ pm corresponding to 0.4 wave numbers. This determines the lower limit on the linewidth of the laser. Several factors, like size of the beam passing through the gain medium and alignment concerns, contribute to broadening of the spectrum.

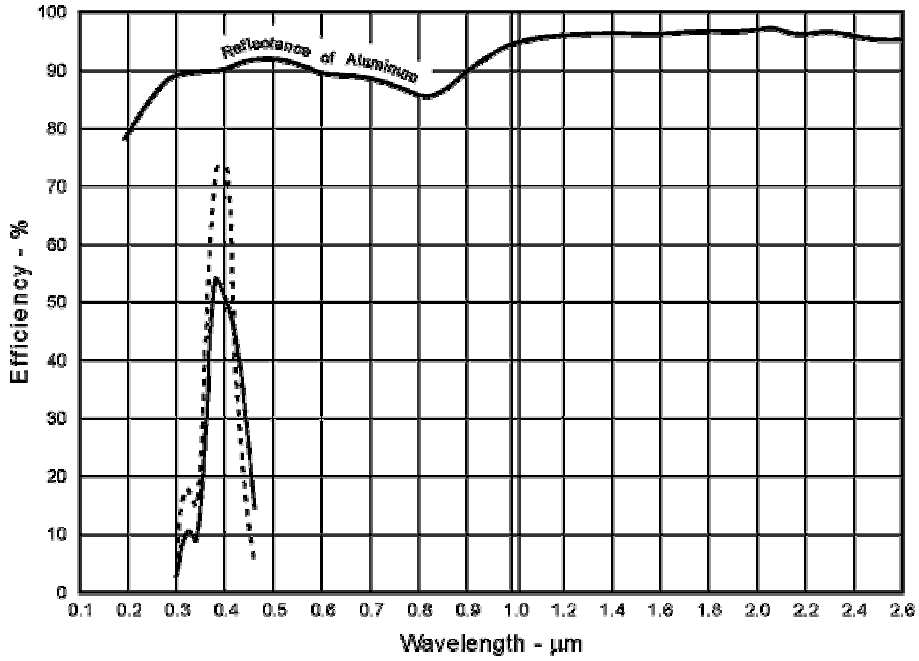

Figure 2.3 Diffraction grating efficiency curve. The bold line represents the efficiency of the grating for p-polarized light. The efficiency is about 50% over our range of operation

In order to illuminate all the grooves of the grating to obtain the above calculated resolution, we expanded the beam falling on the grating using a quad prism beam expander. We aligned the pre-expanded beam emitted by the dye such that it fell in the center of the diffraction grating. This is very important since this ensures that the laser beam is oscillating parallel to the axis of the laser cavity and there are no unwanted reflections from the various surfaces in the cavity. The grating has an efficiency of over 50% throughout our operating range of wavelength. It has an aluminum coating that has over 90% reflectivity in the blue region of the spectrum. The grating forms one end of the laser cavity while the other end is formed by a piece of glass with one side AR coated. The gain in a dye medium is so high that only 4% reflection from the output coupler is sufficient to overcome the losses in the cavity.

In order to optimize the system, we played with the horizontal and vertical alignment of the output coupler and the first beamsplitter, and the rotation of the cylin-

drical lens to maximize the output power. Apart from ensuring high output power, we had to make sure that the beam was not jumping around implying that there is more than one mode oscillating in the lasing cavity.

At one point, we noticed two beams coming out of the cavity instead of one. After playing with the various alignments, we realized that it was due to the angle at which the dye cuvet was aligned. There dye laser beam was getting reflected by the edge of the dye cell facing towards the pump beam. Thus, by changing the angle slightly, we were able to make it square to the output coupler and the grating.

There are a lot of fringes in the beam coming out of the laser cavity. We aligned the laser to the best of our ability to minimize the number of fringes. The output power from the oscillator cavity is 30 mW at the wavelength of maximum efficiency of the gain medium.

The gain medium is the Exalite 411 dye from Exciton, Inc. The solvent specified by the company for this dye is p-dioxane. By nature, dyes are toxic and need special handling. We shall address the issue of the precautions in handling the dye and the solvent later in this chapter. The dye as well as the solvent is colorless. The concentration of the dye in p-dioxane for the oscillator stage, specified by the company is 2.3×10^{-4}moles/L. We were able to verify it by playing with the concentration of the dye to peak up the power of the emitted laser light.

The excited region of molecules is cylindrical in shape within the dye cell. One of the horizontal edges of the cylinder is abrupt since it is the edge of the dye cell but the other edge is not well defined since the penetration of the pump beam into the dye does not end abruptly. However, both the vertical edges of the cylinder are well defined by the size of the pump beam. These edges define a gain region for the laser photons. This gain region controls the divergence of the beam. Exact measurements of the beam size and divergence angle will be shown in the next chapter.

The laser light coming out of the oscillator stage follows its path through the

preamplifier stage.

2.2.3 Preamplifier

The preamplifier stage is simply a gain medium. It is transversely pumped like the oscillator stage and the geometry of this stage is the same as the oscillator stage where the pump beam is reflected off of a beamsplitter and then goes through a cylindrical lens which focuses the beam onto the dye cell. However, we do not need to use an additional beamsplitter since typically an amplifier stage can be pumped much harder than the oscillator stage without bringing in any instability. Also, when we blocked the seed beam, we did not observe any superradiance.

We introduce a delay of a few ns between the time at which the pump beam excites the dye in the oscillator stage and the preamplifier stage. This is done by introducing two 180° prisms in the path of the pump beam going to the preamplifier stage, thus increasing its path length. The delay is important because the laser light takes time to build up within the laser cavity before it passes through the preamplifier stage. Hence, the pump beam delay matches the delay due to the oscillation of light within the laser cavity so that the dye molecules in the preamplifier stage are in the excited state when the dye laser light is passing through it. This stage gives a boost to the laser output power. We maximize the output power by playing with the alignment and concentration of the dye in the solution. The light coming out of this stage also diverges very rapidly in the vertical direction.

Apart from the alignment of the beamsplitter and the cylindrical lens taking the pump beam to the dye cell, the position of the preamplifier dye cell was very important. While the output power increased rapidly as we aligned so that the laser beam passed through the region closer to the edge of the dye cell, there were more fringes in the beam due to diffraction from the edge. Hence, there is a trade off between the output power and beam quality. We chose to focus more on obtaining

a good beam out of the preamplifier cell since we were sending the beam through another amplifier stage which would give us more output power as discussed in the next section. The concentration of the dye solution in the preamplifier stage is the same as the oscillator stage since they are in series and the same solution flows through both dye cells. We obtained about 180mW of power from the preamplifier stage.

2.2.4 Amplifier

Like the preamplifier, this stage is also just a gain medium where stimulated emission occurs due to the dye laser beam going through the excited state molecules. The cuvet in this stage is larger in size than the oscillator or preamplifier stage measuring 50.8mm×17.78mm×21.6mm. This is due to the following reasons: If transversely pumped, the greater the pathlength of a photon through excited state molecules, the greater the amplification. If longitudinally pumped, a bigger pump beam implies greater number of excited molecules which in turn implies a higher saturation power and easier alignment. Thus to facilitate this expansion, the dye cuvet is larger in size.

In our laser, the amplifier stage is longitudinally pumped as shown in Figure 2.4. The advantage of longitudinal pumping is good beam shape and quality. Since the gain in a dye medium is very high, the beam going through a longitudinally pumped dye can be saturated so as to come out with uniform intensity. So if we put in a nice circular beam into a dye gain medium that is longitudinally pumped, we get good circular beam out with uniform intensity. The disadvantage of longitudinal pumping is the difficulty in alignment of the beams.

We did not expand the dye laser beam due to spatial constraints within the laser. We were able to put in only one cylindrical lens between the preamplifier and amplifier stage in order to make the beam circular. By the time the beam enters the amplifier stage, it is about 2.3 mm in diameter. Due to the small size of the dye laser beam, we

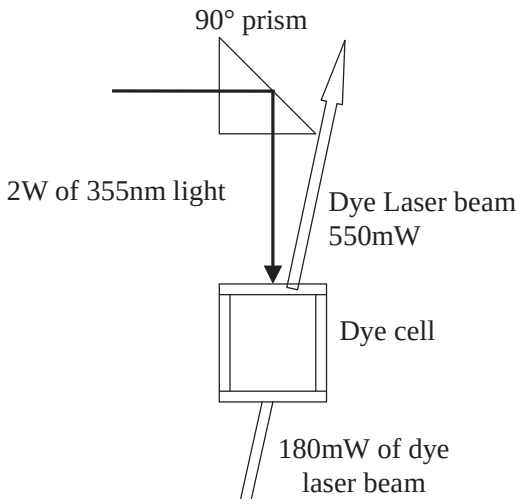

Figure 2.4 Longitudinal pumping. The amplifier stage is longitudinally pumped to obtain good beam quality

reduced the size of the pump beam to half and obtained greater penetration depth.

Since we pump this stage with almost 2W of 355nm light, we obtain tremendous gain and thus more than 550mW of output power. As we are dealing with very high pump powers, it is very important to ensure that the dye is always flowing otherwise there is a danger of burning the dye cell. The next section will talk more about the dye circulator.

All the optics and cuvets are made of fused silica as it has the least amount of absorption in the UV and blue region of the spectrum. The coatings on the optics are specially made to handle the high instantaneous powers that we are dealing with in this laser. The instantaneous power of the pump beam is of the order of a few megawatts and of the dye laser is hundreds of kilowatts.

2.3 Dye Circulator

The dye circulator consists of two sets of motors, pumps, filters and reservoirs, one for the oscillator and preamplifier stage and one for the amplifier stage. The flow

rate of the dye solution is 3.2L/min.

We use 2L reservoirs and there is about 400mL of solution contained within the tubes which makes the total volume of the dye solution = 2.4L. Exciton Inc. specified the lifetime of the dye as 1000 kJ/L for dye concentration of 7×10^{-4} moles/L. The concentration of our oscillator and preamplifier solution is 2.3×10^{-4} moles/L and the concentration of the amplifier stage solution is 6×10^{-5} moles/L. Since we are shining a total of 30 mJ/pulse of pump energy on the oscillator and preamplifier stage, the lifetime of the oscillator/preamplifier solution is $\geq$ 25 million pulses from the pump beam. We use 200 mJ/pulse of pump energy to excite the amplifier stage and so the lifetime of the amplifier solution is about 1 million pulses.The above calculations are done assuming that the lifetime is proportional to the concentration.

Even though we obtained greater output power with a lower concentration of dye in the amplifier stage solution, we maintain a high concentration of 6×10^{-5} moles/L for a longer lifetime of the solution.

We use teflon tubing since the dye and solvent do not affect teflon adversely. We had to put a steel wire throughout the tubes since p-dioxane tends to develop static charge over time as it flows, which can then puncture the tubes (A small section of the tube between the motor and filter did not have steel wiring through it and it developed a puncture within six months of use). Thus we ensure that the solution is grounded at all times.

P-dioxane is volatile and its fumes are known to cause headaches. Thus the dye circulator is kept under a hood. The dye solution is prepared and stored under a hood too. The dye itself is carcinogenic and so we wear protective gloves to handle the dye as well as p-dioxane.

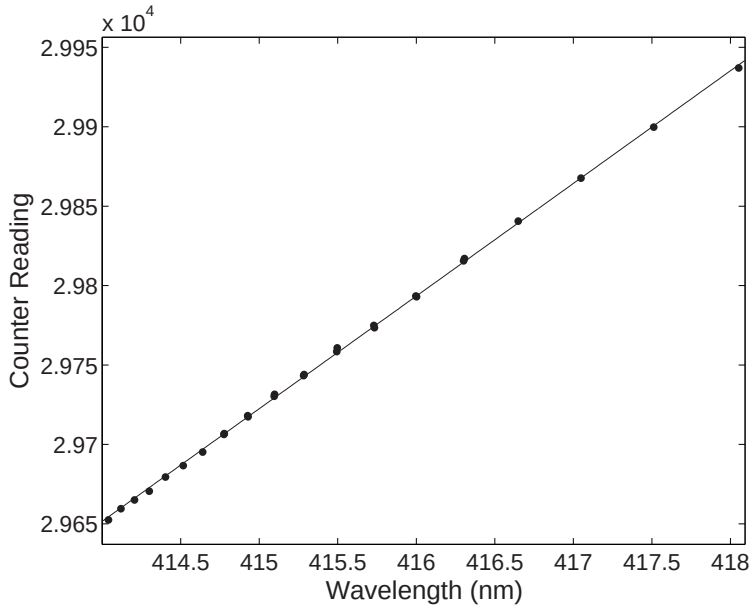

Figure 2.5 Calibration of the counter. We obtained a linear relation between the counter reading and wavelength with slope=70.93 and an intercept=4.042. The dots in the figure represent the estimated center of the Rydberg peaks constituting our data and the solid line is the fit for the calibration of the counter in terms of wavelength

2.4 Computer control

The laser light is tuned by rotating the diffraction grating within the laser cavity. The grating mount is connected to a stepper motor. We can rotate the mount manually by rotating a knob, which is attached to the mount through a system of pulleys. We have also designed a labview program to electronically control the stepper motor. We input our starting wavelength and ending wavelength and the program calculates the number of steps the motor needs to take in order to rotate the grating by the right amount.

The stepper motor is connected to a counter that indicates the wavelength that the laser is emitting. This counter does not directly read the wavelength but shows a number that is a representation of a particular wavelength. A rough estimate of the calibration, correct to a nm, was obtained by observing an auto-ionization peak known to be at 405nm [20] and the peak of the gain curve of the dye specified to

be at 412 nm. An better calibration of the counter was obtained by analyzing the Rydberg atom excitation with the dye laser. Figure 2.5 shows the calibration of the counter. This will be discussed in greater detail in chapter 4.

Chapter 3
Ionization of Strontium

Laser-cooled strontium atoms are photoionized using the pulsed dye laser to make ultracold plasma. The ionization is a two-photon process where one photon from the MOT lasers excites the strontium atoms from the $^1S_0$ state to the $^1P_1$ state and the second photon ionizes the excited atoms as shown in Figure 4.1. Thus the ionization fraction is limited by the number of excited state atoms.

Since ultracold plasma dynamics depend on the plasma density, it is exciting to study the various processes like expansion, thermalization and recombination at different initial plasma densities. One way of changing the plasma density is by varying the ionization fraction. We use the MOT fluorescence signal to monitor the ionization fraction since it is directly proportional to the number of atoms in the MOT, and the shift in the fluorescence is directly proportional to the number of atoms ionized.

Figure 3.2A shows the signal when there are no ions in the MOT and Figure 3.2B shows the MOT fluorescence signal when the atoms are photoionized. The huge peak in both the figures is due to an electronic pickup from the ND:YAG laser which is present whether we shine the photoionizing laser on the atoms or not. The position of this peak coincides with the time at which the atoms are photoionized by the dye laser beam.

As seen in Figure 3.2B, after the photionizing pulse hits the atoms, the fluorescence signal is smaller and this shift corresponds to formation of the plasma. This is because the strontium ions do not scatter the 461nm light that the neutral atoms absorb. If we looked at the signal for a longer time, we would see a gradual decrease in the shift of the signal because of reloading of the MOT. No shift in the fluorescence occurs in Figure 3.2A since no atoms are ionized.

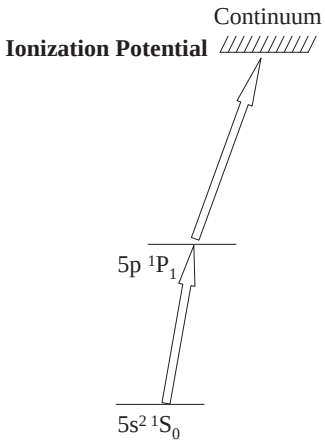

Figure 3.1 Energy levels of strontium. The MOT lasers excite the atoms to the $^1P_1$ state and the dye laser ionizes these excited state atoms

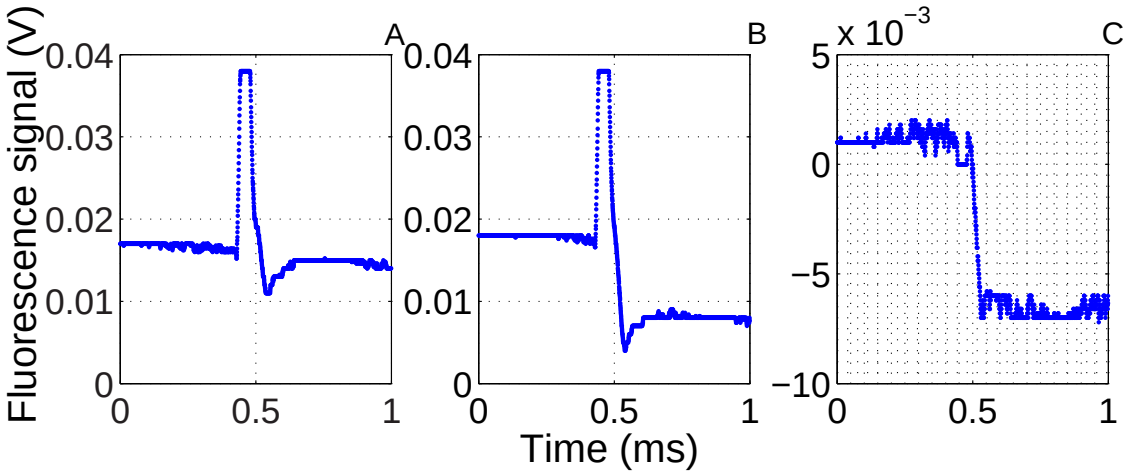

Figure 3.2 MOT fluorescence signal. The MOT fluorescence signal is directly proportional to the number of atoms in the MOT. Figure A is the signal when there are no ions in the MOT. The huge peak is due to electronic pickup from the ND:YAG laser which corresponds to the time of the arrival of the photoionizing pulse. The pickup is present whether we shine the photionizing beam onto the atoms or not. Figure B shows the fluorescence signal when we do photoionize the atoms. The signal on the left of the pulse is before photoionization and on the right is after photoionization has occured. The signal decreases since the ions do not scatter 461 nm light. Figure C is the difference between trace A and B. The ionization fraction is obtained by dividing this signal by the total fluorescence due to the neutral atoms before photoionization. The figure corresponds to an ionization fraction of 0.1

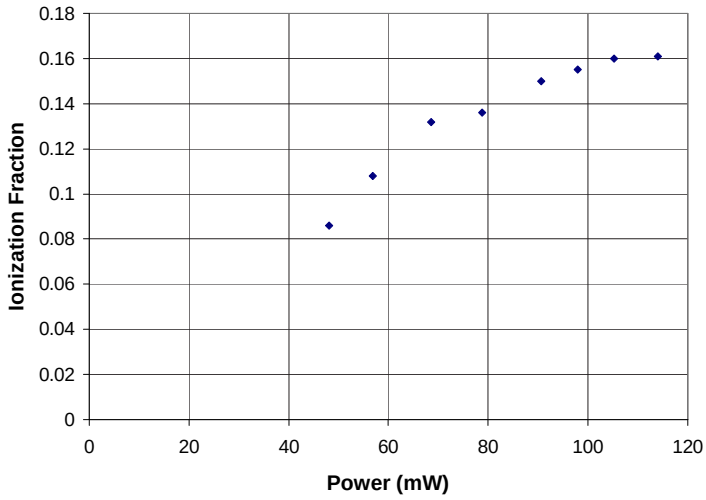

Figure 3.3 We measured the ionization fraction at different output powers from the dye laser to confirm that we had sufficient power to ionize 100% of the excited state atoms. The 412 nm photoionizing beam was 1 cm in diameter

We obtain a quantitative measure of the ionization fraction by subtracting the signal in Figure 3.2A from 3.2B and dividing it by the fluorescence signal from the atoms before photoionization in Figure 3.2B. The difference between the signal before and after photoionization can be seen in Figure 3.2C. The figures show an ionization fraction of 0.41.

3.1 Ionization Fraction versus Power

We wanted sufficient energy in the photoionizing laser beam to ionize all the atoms in the excited $^1P_1$ level [20].

$$n_{ion} = n(^1P_1)[1 - exp(-\sigma\phi_{ph})] \tag{3.1}$$

where,n_{ion} is the density of ions, $n(^1P_1)$ is the density of excited state atoms, σ is the photoionization cross section and ϕ_{ph} is the photons per unit area in the photoionizing

beam. Hence, the fraction of excited state atoms photoionized is:

$$\frac{n_{ion}}{n(^1P_1)} = [1 - exp(-\sigma\phi_{ph})] \tag{3.2}$$

With a photoionization cross section of 300Mb [20] and a 15 mJ/cm^2 beam, we can ionize more than 95% of the excited state atoms.

We studied the ionization fraction at different output powers of the photoionizing dye laser to check if we had sufficient power to photoionize all the excited state atoms. The results are plotted in Figure 3.4, where we can see that we are saturating the atoms with the photoionizing light. The maximum ionization fraction is 0.16 because of the small fraction of excited state atoms. We have obtained ionization fractions of up to 0.41 by putting an on-resonance beam at 461 nm through the MOT which ensured a greater number of excited state atoms which could be photoionized. Hence, we concluded that we had sufficient power to obtain the desired plasma densities for our experiments.

To reduce the plasma density, we use neutral density filters in the path of the dye laser beam to decrease the amount of light going to the atoms. We have one filter wheel with 5 filters of different optical densities. Hence, we can study the dynamics of the ultracold plasma at different initial densities.

3.2 Ionization Fraction versus Wavelength

Once we were sure that we had sufficient power to photoionize all the excited state atoms, we measured the ionization fraction at various wavelengths. The wavelengths were obtained by calibrating the counter readings which is explained in the next chapter. During this study, we observed a huge peak, known to be the auto-ionizing peak at 405 nm [20]. Autoionization refers to the following process: Two electrons are excited to a quasi-bound autoionizing level that ionizes through one electron coming down to the ground state, giving off its energy, while the other electron is released.

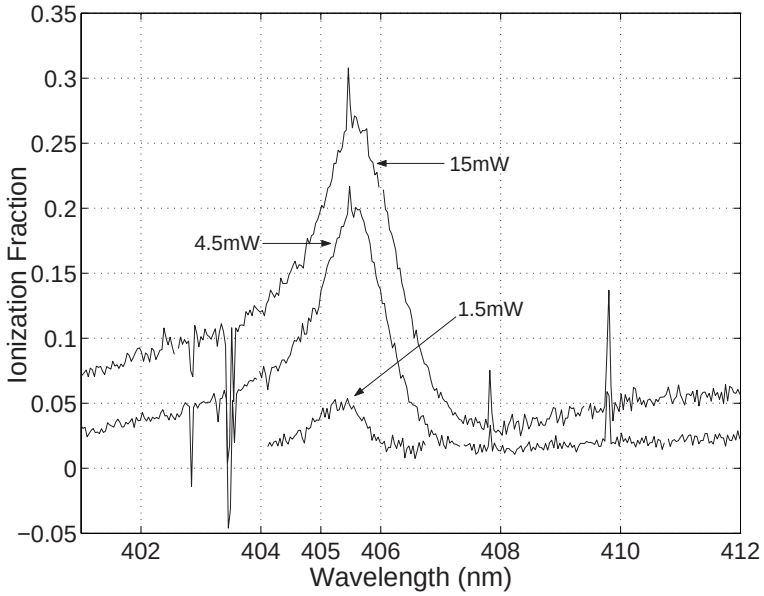

Figure 3.4 Ionization fraction at different wavelengths. In order to get an estimate of the photoionization cross section, we measured the ionization fraction at different wavelengths. We obtained the autoionizing peak during this study. (The calibration of the counter to obtain wavelength in nm will be discussed in the next chapter)

Figure 3.5 shows the autoionization peak for different plasma densities. We took the data at different powers, with a 1 cm diameter beam, to show saturation effects. We can see that the peak for 4.5 mW power of dye laser has about 3 times greater amplitude than the one at 1.5 mW, as expected. However the amplitude of the peak at 15 mW power of dye laser is only marginally larger than the one at 4.5 mW. This is because we are saturating the atoms. This saturation also causes broadening of the peak since the signal goes up proportionally in the wings of the peak . The data for the autoionizing peak looks similar to the one in [20].

We fit the autoionization peak for 4.5 mW to the Fano profile [21]:

$$\sigma(\epsilon) = \sigma_a[\frac{(q+\epsilon)^2}{1+\epsilon^2}] + \sigma_b \tag{3.3}$$

Here,

$$\epsilon = \frac{(E - E_R)}{\frac{1}{2}\Gamma} \tag{3.4}$$

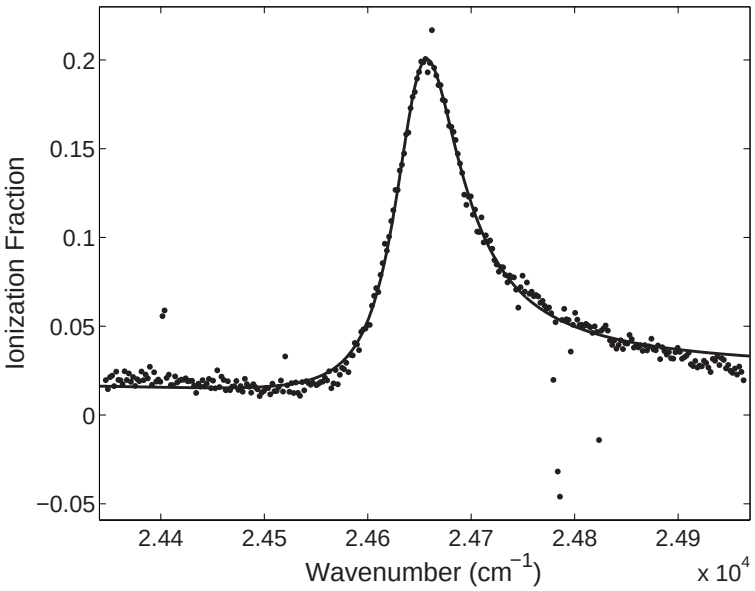

Figure 3.5 Autoionization peak. We fit the ionization fraction data to the Fano profile to obtain the position of the autoionizing level which helped us verify the goodness of our calibration of the counter which is discussed in the next chapter

is the difference between the incident photon energy E and the resonance energy E_R corresponding to the autoionizing level; Γ is the width of the line; $\sigma(\epsilon)$ is the absorption cross section for photons of energy E; σ_a refers to some background cross section and σ_b is an offset.

The fit parameters obtained from the Fano profile are: $E_R = 24649.2 \pm 0.46$ cm^{-1}, $q = 5.057 \pm 0.125$, $\Gamma = 77.32 \pm 0.505$ cm^{-1}. The cross section σ reaches its maximum value at:

$$E_{max} = E_R + \frac{1}{2}(\Gamma/q) \tag{3.5}$$

and its minimum at:

$$E_{min} = E_R - \frac{1}{2}(\Gamma q) \tag{3.6}$$

Using the above equations, we obtain $E_{max} = 24656.8$ cm^{-1} and $E_{min} = 24453.7$ cm^{-1}. Figure 4.6 shows that the fit values correspond well with our measured data. The wavenumbers in the figure are obtained after calibration of the counter reading

which is discussed in the next chapter.

The Fano parameters obtained by Mende et al. [20] are: E_R=24678.3 cm^{-1}, q= 5.8 and Γ = 56.2 cm^{-1}. We notice a difference of 28.9 cm^{-1} between their and our value of E_R which can be accounted for by experimental error. The stepper motor circuit was not reliable for long scans of the spectrum. The counter was missing steps and so the counter reading recorded by the labview program did not correspond well with the actual readings on the counter over the long scan. However, the difference in the q parameter indicates to us that there is some error in our measurement. Although we fit the 4.5 mW peak to the Fano profile, saturation could still be a problem and that could be the reason why the width of our profile is larger.

When we look carefully at the three peaks in Figure 3.5, we notice that the center of the smallest peak does not line up with the center of the other two peaks. Even though this shift looks small on the wavelength scale, it amounts to about 20 wavenumbers. This indicates a problem in reproducibility of the data which can be traced back to the faulty stepper motor circuit. We were also limited by the quality of our wavelength calibration. This will be discussed in greater detail in the next chapter.

Chapter 4
Characterization of the Laser

We characterized the dye laser by looking at the beam quality, output power and the spectrum.

4.1 Beam Quality

A pulsed dye laser is typically multimode unless some mode selection methods are employed. Since we are not using any such methods in the dye laser, the beam is a mixture of various TEM modes. There are a lot of fringes on the beam due to diffraction from the edge of the dye cell. We expand the beam and use the central portion of the beam, which has a uniform intensity, to ionize the atoms.

The beam expands unevenly in the two axis, so we used cylindrical and spherical lenses to control the expansion such that the beam was 1 cm in diameter when it passed through the MOT. In order to estimate the focal length of the lenses required for the purpose, we measured the beam waist of the light coming out of the oscillator cavity to obtain the beam divergence.

The beam waist was measured using the knife edge method where a sharp edge is used to find portions of the beam where the intensity is 0.1 and 0.9 times the total intensity. Initially the knife edge blocks the laser beam completely. The data is taken by moving the knife edge in small increments to gradually allow more and more light from the laser to hit the power meter. The plots of these measurements indicated that even though the dye laser beam is a mixture of various TEM modes, most of it is TEM_{00} mode. Figure 4.1 shows a typical measurement taken at a distance of 385 mm from the output coupler. Hence, we used the following formula to extract the spot size at that distance.

$$\omega = 0.552 * \sqrt{2} * (\chi_{10} - \chi_{90}) \tag{4.1}$$

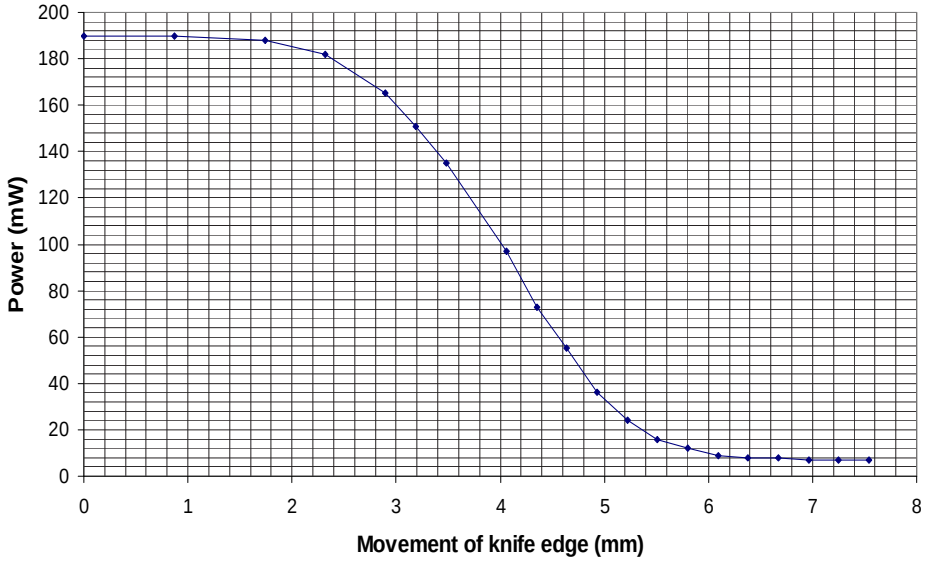

Figure 4.1 Beam waist measurement. We use the knife edge method to measure the beam waist. This particular measurement was done for the vertical beam diameter at a distance of 385mm from the output coupler

where χ_{10} and χ_{90}, respectively, are positions of the knife edge at which the laser power is 10% and 90% of its maximum. Five sets of measurements were taken at various distances from the output coupler for the horizontal and vertical spot size. The next step was to fit this data to the following formula to obtain the beam waist and its position:

$$\omega^2(z) = \omega_0^2[1 + (\frac{\lambda z}{\pi\omega_0^2})^2] \tag{4.2}$$

where ω is the spot size at distance z from the waist, λ is the wavelength of light, ω_0 is the beam waist. We apply (4.2) to the vertical and horizontal beam waist separately since they do not lie at the same place. This also enabled us to calculate the beam divergence:

$$\theta = \frac{\lambda}{\pi\omega_0} \tag{4.3}$$

For $\lambda = 412$ nm, we find that the horizontal waist measures 0.05 ± 0.006 mm and has a divergence of 2.6 mrad. The vertical waist is $0.03 \pm .002$ mm with a divergence of 4.7 mrad. The position of both the beam waists were approximated to be within the

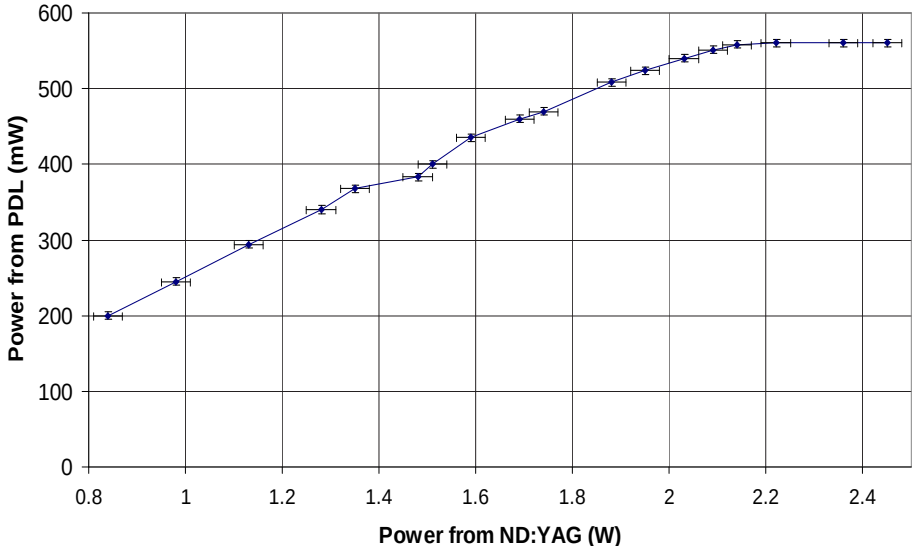

Figure 4.2 Saturation curve of dye laser. The measurement of the output power from PDL at different input powers from the pump laser ensured that we were saturating the laser dye

oscillator dye cell with an uncertainty of less than 3 cm for the vertical waist and an uncertainty of about 6 cm for the horizontal waist.

Equipped with the knowledge of the beam divergence, we installed a cylindrical lens of focal length 200 mm between the preamplifier and amplifier dye cell to limit the expansion in the major axis and make the beam circular before it passes through the amplifier stage.

Since the laser cavity consits of a flat piece of glass on one side and a diffraction grating on the other, the beam waist and divergence are determined by the excited state region in the oscillator cavity. The excited regions in the preamplifier and amplifier stages are larger in size than the laser beam going through them. Hence, they do not affect the size and position of the beam waist appreciably.

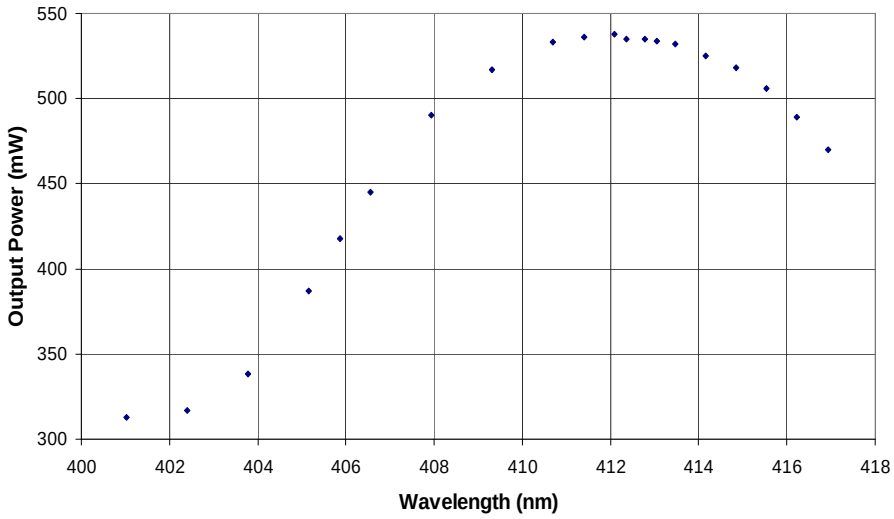

Figure 4.3 Output Power from PDL vs. Wavelength. We measured the output power from dye laser at different wavelengths and reproduced the gain curve of the dye provided by Exciton, Inc

4.2 Output Power

Laser dyes have tremendous gain and so we need high pump power to saturate the gain medium. We varied the pump power and measured the corresponding output power from the dye laser using a power meter. Figure 4.2 shows that we were able to saturate the dye in our photoionizing laser and thus obtain the maximum output power. The gain curve of the dye as seen in Figure 4.3 followed the one provided by Exciton, Inc.

4.3 Rydberg Series

We excited the Rydberg series of strontium using the pulsed dye laser. This series helped us calibrate the counter attached to the grating mount and estimate the laser

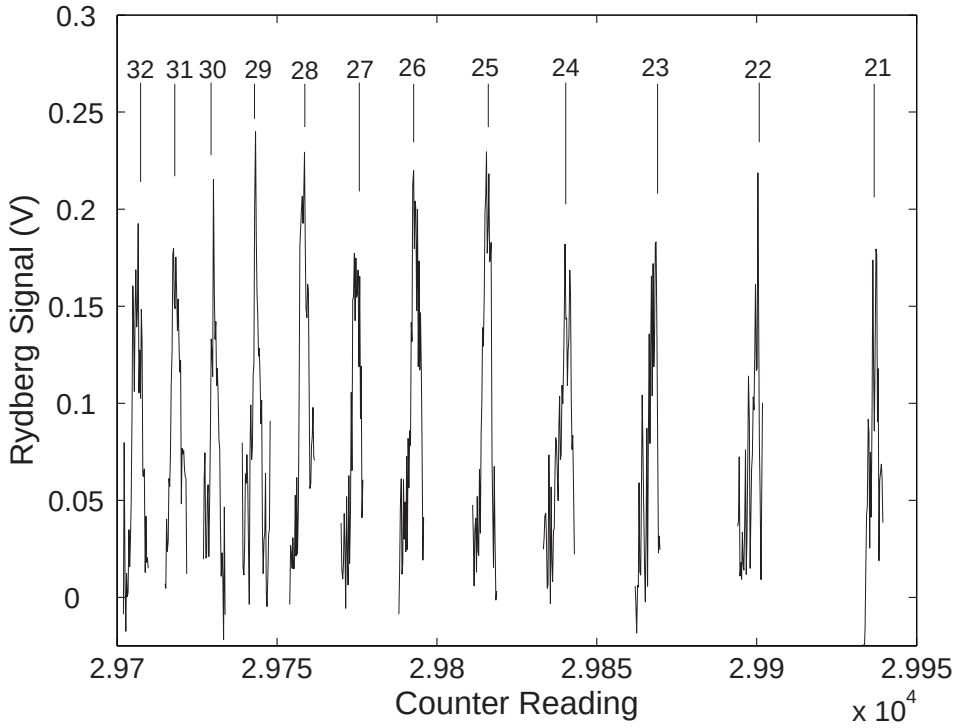

Figure 4.4 Rydberg levels. The figure shows the Rydberg series obtained by exciting the $^1P_1$ level atoms using the dye laser. The numbers in the figure indicate the quantum number corresponding to the peak obtained after calibrating the counter

linewidth.

The strontium atoms were cooled and trapped, with the 461 nm light, to a temperature of a few mK before we excited them to the Rydberg levels. The Rydberg atoms collide and spontaneously ionize themselves to form a plasma [10]. Hence, if we measure the MOT fluorescence signal, there would be a decrease in the fluorescence when we excite the atoms to a Rydberg level, since the ions do not scatter the 461 nm light. This enabled us to take the Rydberg series data with the same experimental procedure as described in chapter 3. Figure 4.4 shows the Rydberg peaks obtained when we tuned the laser from 414 - 417 nm.

We used the Rydberg series data to obtain an estimate of the linewidth of the laser. We understand that the linewidth of the laser must be smaller than the narrowest

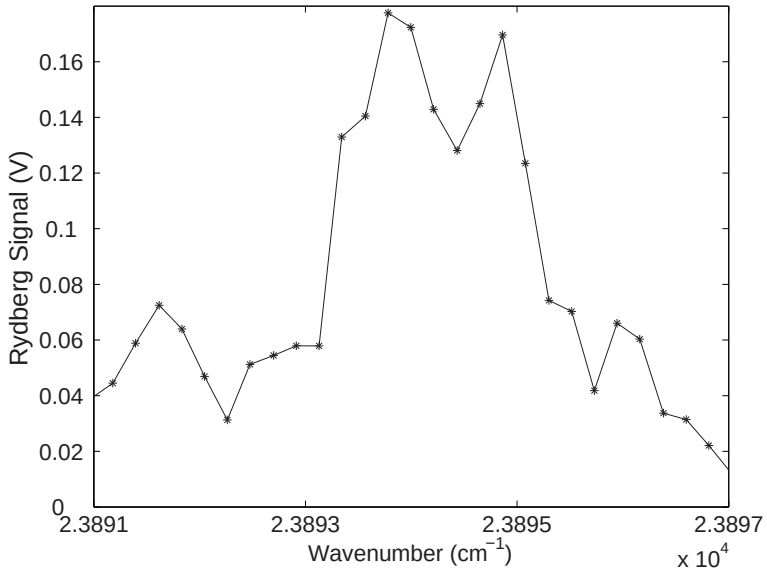

Figure 4.5 Linewidth of the dye laser. The figure shows the narrowest Rydberg peak obtained using the pulsed dye laser. The linewidth of the laser must be smaller than the width of this peak. Hence, we estimated the linewidth of the laser to be ≤ 2 wavenumbers

peak we obtained in the entire spectrum. Figure 4.5 shows the narrowest Rydberg peak in our data set, through which we estimated the upper limit on the linewidth of the pulsed dye laser to be 2 wavenumbers.

We began the process of analyzing the data by estimating the uncertainties that we could obtain by simply looking at the data set. The linewidth of the laser is the most obvious limit on our resolution of the Rydberg levels. Figure 4.6 shows the same Rydberg peak taken at two different plasma densities. Fitting the data to a Gaussian profile showed that the center peaks are shifted by about half a counter reading due to collisions. Since Rydberg atoms spontaneously ionize themselves to form a plasma, there might be a small field generated by the ions and electrons which can cause shifts in the Rydberg levels. However, we cannot be definite that there is a shift in the peak since our data is noisy. Also, our stepper motor circuit could not be trusted enough to quantify such a small shift. The peak taken at higher plasma density has a greater width than the one at lower density which implies that collisions

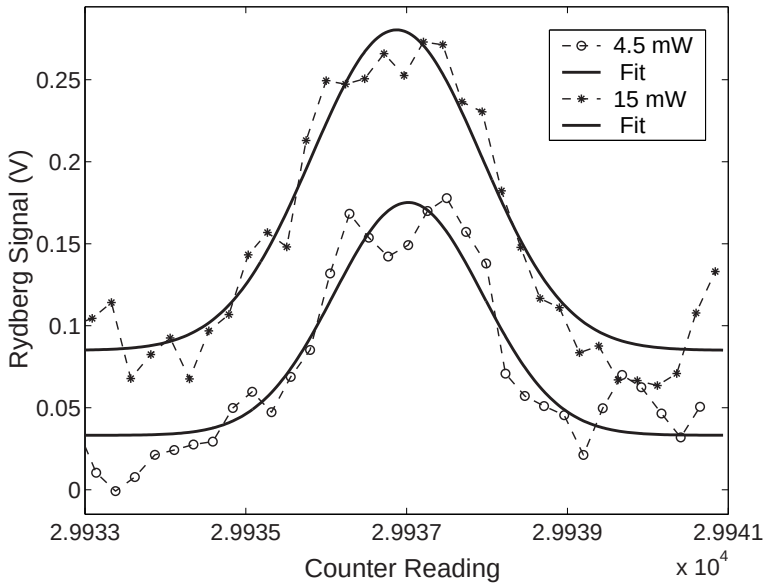

Figure 4.6 Shifts in the Rydberg peak. We fit the Rydberg peaks taken at two different plasma densities, using a 1 cm diamter photoionizing beam, to a Gaussian profile and noticed that the centers are shifted due to collision of the atoms. This collision leads to spontaneous photoionization of the Rydberg atoms to form plasma. The plasma can generate a small field which can also cause the levels to shifts

play a role in broadening the peaks.

Another uncertainty came about by the observation that the counter readings recorded by the labview program did not always match the actual readings on the counter. This implied that the counter was skipping steps and the stepper motor circuit was not reliable.

Keeping these points in mind, we decided to read the center of each peak by eye instead of fitting them to a Gaussian since the error would be negligible compared to our uncertainties. We estimated the uncertainties to be one quarter the width of the peak since the signal to noise ratio was about 4.

The next step in our data analysis was to determine the quantum number corresponding to each Rydberg peak. For a rough estimate, we decided to compare the difference in wavenumber between adjacent peaks obtained experimentally and theoretically. However, this required a rough calibration of the counter so that we could

convert the counter readings to wavenumbers.

The dye laser manual provided by Quanta Ray states that the counter reading = (wavelength ($\mathring{A}$) of light coming out of the laser)*(order of diffracted light sent back to the laser). Since we had realigned the laser using new optics, we needed to recalibrate the counter. However, to a first approximation, it was sufficient to use the relation mentioned in the manual, which helped us estimate that a difference of one counter reading is equivalent to a difference of one wavenumber. Thus, we were able to assign quantum numbers to the Rydberg peaks as shown in Fig. 4.4.

After assigning the quantum numbers, we refined our data analyzing process to obtain more accurate calibration. We assumed the relation between the counter reading and wavelength to be the following:

$$C = m * (\lambda + o) \tag{4.4}$$

where, C is the counter reading, m is the multiplicative factor, λ is the wavelength in nm and o is the offset. The energy of a Rydberg level is given by:

$$E(cm^{-1}) = \frac{Ry}{(n-\delta)^2} \tag{4.5}$$

where, Ry = 109736.637 cm^{-1} is the Rydberg constant for strontium, n is the quantum number and δ is the quantum defect. We used [11] as our reference data to obtain reasonable values for the quantum defects. Looking at Esherick's data, we noticed that the n^1S_0 and $(n+1)^1D_2$ Rydberg levels lie less than a wavenumber away from each other. The dye laser was unable to resolve these levels and the width of the peaks in our data ranged from 2-4 wavenumbers.

The propensity rule says that transitions in which the orbital quantum number increases are stronger [22], however, we assumed equal oscillator strengths for the $^1S_0$ and $^1D_2$ transitions since we do not have a quantitative guide to the relative strengths and the error introduced by this assumption is not appreciable compared to our

uncertainties. Hence, for our calibration purposes, we assume that the wavenumber corresponding to each Rydberg peak follows the relation:

$$E(cm^{-1}) = Ry * [\frac{1}{((n+1)-\delta_D)^2} + \frac{1}{(n-\delta_S)^2}] \tag{4.6}$$

and then we convert wavenumber to wavelength:

$$\lambda(nm) = \frac{10^7}{E(cm^{-1})} \tag{4.7}$$

where, $\delta_D = 2.35$ is the average quantum defect for the $^1D_2$ levels and $\delta_S = 3.269$ is the average quantum defect for the $^1S_0$ level. The difference in the energy calculated using the actual quantum defect, corresponding to a particular Rydberg level, and an average defect was negligible compared to our uncertainties.

Combining (2.4), (2.5) and (2.6), we obtain a relation between the counter reading and wavelength. We fit the experimental counter readings using this relation for different quantum numbers to obtain the best fit for 'm' and 'o'. Having a rough estimate of the quantum numbers to start with greatly reduced the number of iterations required to obtain the best fit. The results of the fit were: m = 70.93 ± 0.25, o = 4.042 ± 1.48. Figure 2.5 shows the data and the fit.

Figure 4.8 shows the residues with the errors. The error bars were drawn over the range of (data + uncertainty) to (data - uncertainty). There are several reasons why the fit is not perfect. Our assumption of a linear calibration of the counter might not be true, since we see a systematic error in our fit. There are some unresolved peaks in the spectrum as we go to higher quantum levels. This explains the huge error bars on the first few data points. Also, the peaks are broad and have a weird shape due to noise, and the fact that they are a mixture of the $^1S_0$ and $^1D_2$ levels.

We were limited in our data taking process by the stepper motor circuit which controls the rotation of the grating mount. While the circuit worked fine for small scans of the laser, we ran into trouble trying to scan the whole spectrum. This was because the counter was skipping steps every now and then during the scan. Hence,

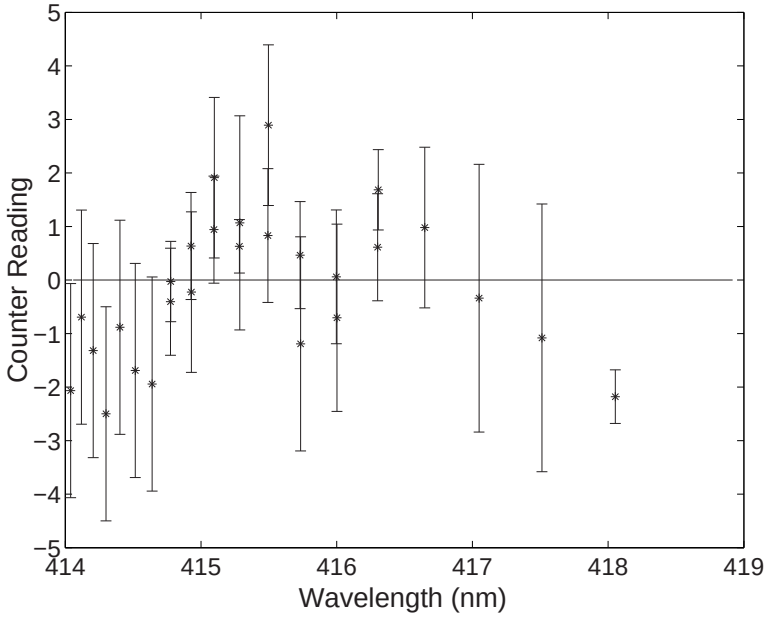

Figure 4.7 Residue from the fit of the counter readings. The figure shows the residues, with uncertainties, from the fit of the counter readings. There seems to be a systematic error in the calibration of the counter

the counter reading recorded by the labview program did not correspond well with the actual reading on the counter.

This greatly affected the reliability and reproducibility of the autoionization peak. Referring to our discussion of the Fano parameters in chapter 3, we noticed a difference of about 29 wavenumbers in the resonance energy between our fit and [20]. Also, the peaks were shifted by about 20 wavenumbers when reproduced.

In order to calibrate the counter throughout the entire spectrum of the dye laser, we included the autoionization peak data in the fit. This gave us new fit parameters which made our Rydberg data look bad. We did not trust these fit parameters since there is a large uncertainty in the autoionization peak data. This is because it is a very broad peak, broadened further by saturation effects, and we were trying to split the peak to find a very narrow feature. Besides, our doubt about the linear relation between the counter readings and wavelengths adds greatly to the uncertainty since

this peak lies very far from the Rydberg levels in the spectrum.

We have not reached our goal of a calibration good to ≤ 1 wavenumber. However, the current calibration is good enough for our experiments [23] since we are exciting the atoms to temperatures of 68K or more. We will definitely require a better calibration in order to get closer to the ionization threshold in the experiments. This constitutes the future work that needs to be done on the dye laser system.

4.4 Future Plans and prospects

The pulsed dye laser has proven to be a robust system for photoionizing laser-cooled strontium atoms to make an ultracold plasma. The Exallite 411 dye has a much longer lifetime than typical laser dyes which enabled us to do ultracold plasma experiments over long periods of time.

While this is a good start, there is much room for improvement. We need to revisit the data and apply better tools for analysis in order to obtain a function which relates the counter reading and wavelength over the entire spectrum.

We have fixed the circuit and it works well for long scans too. This will greatly reduce our uncertainties in future experiments. We intend to measure the ionization fraction at different wavelengths again and revisit the fano fit.

We noticed that our data was broadened by collisions at high plasma densities. Hence, we would like to work at much lower densities to obtain narrower Rydberg peaks. But we were not able to obtain a distinguishable signal in the MOT fluorescence at very low plasma densities.

Since we are equipped with an MCP in the vacuum chamber, which detects individual electron signals, we can obtain large signals at very low plasma densities. We will use the method of pulsed field ionization for detecting the Rydberg levels. We were limited in using this method earlier since our signals were being affected greatly by the stray fields in the vacuum chamber. Also, we were not able to ramp the large

fields, required to ionize the deeply bound levels, fast enough to avoid stark shifts.

With modifications to the chamber, we can make improvements on both the things and obtain more accurate data which will enable us to calibrate our counter and obtain a better estimate of the laser linewidth.

References

1. T. C. Killian, S. Kulin, S. D. Burgerson, L. A. Orozco, C. Orzel, and S. L. Rolston. "Creation of an Ultracold Neutral Plasma" *Phys. Rev. Lett.* **83** 4776 (1999).

2. H. J. Metcalf and P. v. d Straten *Laser Cooling and Trapping.* Springer, New York, first edition (1969).

3. S. Kulin, T. C. Killian, S. D. Burgerson, and S. L. Rolston. "Plasma Oscillations and Expansion of an Ultracold Neutral Plasma" *Phys. Rev. Lett.* **85** 318 (1999).

4. T. C. Killian, M. J. Lim, S. Kulin, R. Dumke, S. D. Burgerson, and S. L. Rolston. "Formation of Rydberg Atoms in an Expanding Ultracold Neutral Plasma" *Phys. Rev. Lett.* **86** 3759 (2001).

5. M. S. Murillo "Using Fermi Statistics to Create Strongly Coupled Ion Plasmas in Atom Traps" *Phys. Rev. Lett* **87** 115003 (2001).

6. S. G. Kuzmin, and T. M. O'Neil. "Numerical simulation of ultracold plasmas" *Phys. Plas.* **9** 3743 (2002).

7. F. Robicheaux, and James. D. Hanson "Stimulated expansion of an ultra-cold, neutral plasma" *Phys. Plas.* **10** 2217 (2003).

8. S. Mazevet, L. A. Collins, and J. D. Kress "Evolution of Ultracold Neutral Plasmas " *Phys. Rev. Lett.* **88** 55001 (2002).

9. S. Ichimaru *Rev. Mod. Phys.* **54** 1017 (1982).

10. M. P. Robinson, B. Laburthe Tolra, Michael W. Noel, T. F. Gallagher, and P. Pillet "Spontaneous Evolution of Rydberg Atoms into an Ultracold Plasma" *Phys. Rev. Lett.* **85** 4466 (2000).

11. Peter Esherick "Bound, even-parity J = 0 and J = 2 spectra of Sr" *Phys. Rev. A* **15** 1920 (1977).

12. P. P. Sorokin, and J. R. Lankard "Stimulated emission observed from an organic dye, chloro-aluminium phthalocyanine" *IBM J. Res. Develop.* **10** 162 (1966).

13. F. P. Schafer, W. Schmidt, and J. Volze "Organic dye solution laser" *Appl. Phys. Lett.* **9** 306 (1966).

14. M. L. Spaeth, and D. P. Bortfeld "Stimulated emission from polymethine dyes" *Appl. Phys. Lett.* **9** 179 (1966).

15. D. J. Bradley, G. M. Gale, M. Moore, P. D. Smith "Longitudinally pumped, narrow-band continuously tunable dye laser" *Phys. Lett.* **26A** 378 (1968).

16. F. P. Schafer, and H. Muller "Tunable dye ring-laser" *Opt. Commun.* **2** 407 (1971).

17. T. W. Hansch "Repetitively pulsed tunable dye laser for high resolution spectroscopy" *Appl. Opt.* **11** 895 (1972).

18. B. H. Soffer, and B. B. McFarland "Continuously tunable, narrow-band organic dye lasers *Appl. Phys. Lett.* **10** 266 (1967).

19. F. J. Duarte, and Lloyd W. Hillman *Dye Laser Principles With Applications.* Academic Press, New York, first edition (1990).

20. W. Mende, K. Bartschat, and M. Kock "Near-threshold photoionization from the Sr I (5s5p) $^1P_1^0$ state" *J. Phys. B* **28** 2385 (1995).

21. T. K. Fang, and T. N. Chang "Determination of profile parameters of a Fano resonance without an ultrahigh-energy resolution" *Phys. Rev. A* **57** 4407 (1997).

22. Hand. A. Bethe and Edwin. E. Salpeter *Quantum Mechanics Of One- And Two-Electron Atoms.* Plenum Publishing Corporation, New York, first edition (1977).

23. C. E. Simien, Y. C. Chen, P. Gupta, S. Laha, Y. N. Martinez, P. G. Mickelson, S. B. Nagel, and T. C. Killian *Using Absorption Imaging to Study Ion Dynamics in an Ultracold Neutral Plasma.* http://www.arxiv.org/PScache/physics/pdf/0310/0310017.pdf (Oct 2003)